Published in final edited form as:
Magn Reson Med. 2010 April ; 63(4): 1031–1043. doi:10.1002/mrm.22290.

Gene Expression Profiling Reveals Early Cellular Responses to Intracellular Magnetic Labeling with Superparamagnetic Iron Oxide Nanoparticles

Dorota A. Kedziorek[1,4,†], **Naser Muja**[1,4,†], **Piotr Walczak**[1,4], **Jesus Ruiz-Cabello**[1,4,6], **Assaf A. Gilad**[1,4], **Chunfa C. Jie**[5], and **Jeff W. M. Bulte**[1,2,3,4,*]

[1] Russell H. Morgan Department of Radiology and Radiological Science, Division of MR Research, The Johns Hopkins University School of Medicine, Baltimore, Maryland, USA

[2] Department of Biomedical Engineering, The Johns Hopkins University School of Medicine, Baltimore, Maryland, USA

[3] Department of Chemical & Biomolecular Engineering, The Johns Hopkins University School of Medicine, Baltimore, Maryland, USA

[4] Cellular Imaging Section and Vascular Biology Program, Institute for Cell Engineering, The Johns Hopkins University School of Medicine, Baltimore, Maryland, USA

[5] Institute for Basic Biomedical Sciences, The Johns Hopkins University School of Medicine, Baltimore, Maryland, USA

[6] Ciber de enfermedades respiratorias, Instituto de Estudios Biofuncionale, Universidad Complutense de Madrid, Madrid, Spain

Abstract

With MRI (stem) cell tracking having entered the clinic, studies on the cellular genomic response toward labeling are warranted. Gene expression profiling was applied to C17.2 neural stem cells following superparamagnetic iron oxide/PLL (poly-L-lysine) labeling over the course of 1 week. Relative to unlabeled cells, less than 1% of genes (49 total) exhibited greater than 2-fold difference in expression in response to superparamagnetic iron oxide/PLL labeling. In particular, transferrin receptor 1 (*Tfrc*) and heme oxygenase 1 (*Hmox1*) expression was downregulated early, whereas genes involved in lysosomal function (*Sulf1*) and detoxification (*Clu*, *Cp*, *Gstm2*, *Mgst1*) were upregulated at later time points. Relative to cells treated with PLL only, cells labeled with superparamagnetic iron oxide/PLL complexes exhibited differential expression of 1399 genes. Though these differentially expressed genes exhibited altered expression over time, the overall extent was limited. Gene ontology analysis of differentially expressed genes showed that genes encoding zinc-binding proteins are enriched after superparamagnetic iron oxide/PLL labeling relative to PLL only treatment, whereas members of the apoptosis/ programmed cell death pathway did not display increased expression. Overexpression of the differentially expressed genes *Rnf138* and *Abcc4* were confirmed by quantitative real-time polymerase chain reaction. These results demonstrate that, although early reactions responsible for iron homeostasis are induced, overall neural stem cell gene expression remains largely unaltered following superparamagnetic iron oxide/PLL labeling.

*Correspondence to: Jeff W. M. Bulte, Ph.D., Department of Radiology, The Johns Hopkins University School of Medicine, 217 Traylor Bldg, 720 Rutland Ave, Baltimore, MD 21205-2195. jwmbulte@mri.jhu.edu.
†These authors contributed equally to this work.

Keywords

superparamagnetic iron oxide; MR contrast agent; magnetic resonance imaging; iron metabolism; cell tracking; cell therapy; microarray

Intracellular uptake of superparamagnetic iron oxide (SPIO) nanoparticles enables noninvasive in vivo MRI of the delivery and biodistribution of cellular therapeutics. Feridex I.V.®, an injectable solution of dextran-coated ferumoxide for hepatic and splenic imaging (1), has been widely applied to label a wide variety of cells and has undergone initial phase I/II testing for dendritic cells in melanoma patients (2), neural stem cells (NSCs) in traumatic brain injury (3), and for pancreatic islet grafts in type I diabetic patients (4). Given the promise of cell therapy and the anticipated pivotal role of clinical MRI cell tracking for real-time delivery and assessment of initial biodistribution, the compatibility and safety of Feridex® labeling must be assured (5).

Several in vitro and in vivo studies have demonstrated that cell viability, differentiation, and proliferation are normal in SPIO-labeled cells (2,6,7). However, reduced synthesis of collagen and extracellular matrix following the induction of chondrogenesis in Feridex® -(8,9) or Resovist- (10) labeled bone marrow–derived MSC has been reported and immunomodulatory effects have been encountered for SPIO-labeled macrophages and their interactions with T cells (11). Recently, the use of acidic medium (pH 4.5, sodium citrate chelate) modeling the pH of the lysosomal compartment has been shown to release Fe^{3+} from iron oxide nanoparticles (12), indicating that retention of SPIO within this compartment could elevate cytosolic Fe^{3+} concentration. In support of this hypothesis, coordinated changes in the expression of genes encoding iron sequestration proteins, transferrin receptor 1, and ferritin are induced in HeLa cells and human MSCs following SPIO labeling (13), indicative of posttranscriptional regulation of gene expression by iron regulatory proteins (IRPs; IRP1 and IRP2) in adaptation to increased cytosolic Fe^{3+} concentration (14).

In conditions where iron homeostasis is not maintained, increased intracellular Fe^{3+} can contribute to Fe^{2+}-catalyzed oxidative damage to nucleic acids, proteins, and lipids (15). Because the signaling properties of iron are not accounted for by routine histochemical detection of cellular markers, complementary assays of intracellular processes, including signal transduction analysis, proteomic studies, and gene expression profiling, are essential for complete characterization of the response of a specific cell type to SPIO labeling prior to transplantation. The multipotent NSC line C17.2 has been widely applied as cell therapy in experimental models of CNS disease (16,17), and the migratory properties of this cell line have been characterized using MRI cell tracking (18,19). In this study, we have labeled C17.2 NSCs with Feridex® (Bayer Healthcare Pharmaceuticals; 25 μg/mL) and the transfection agent poly-L-lysine (PLL) and examined the effect of labeling on gene expression over the course of 1 week in vitro. The present results are directly relevant to current safety considerations in clinical MRI cell tracking trials.

MATERIALS AND METHODS

C17.2 NSC Culture and Labeling

The *LacZ*-expressing mouse NSC cell line C17.2 was cultured in Dulbecco's modified Eagle's medium containing 4.5 mg glucose/mL, 10% fetal bovine serum, 5% horse serum, 1% L-glutamine, 100 IU/mL penicillin, 100 μg/mL streptomycin, and 0.025 μg/mL amphotericin B (Invitrogen, Carlsbad, CA). For cell labeling, 25 μg Fe/mL ferumoxide formulation (Feridex I.V.®, Bayer Healthcare Pharmaceuticals) and PLL hydrobromide

(Mw = 388 kDa; Sigma, St. Louis, MO) at a concentration of 375 ng/mL was incubated in culture medium at room temperature for 1 h (9). The SPIO-PLL-complexed medium was then added to C17.2 NSCs and incubated for 24 h. To control for potential effects induced by the transfection agent PLL alone (without SPIO complexation), cells cultured in parallel were incubated overnight with PLL (375 ng/ mL). C17.2 NSCs were labeled with SPIO/PLL or treated with PLL only on day 1, 4, 6, or 7 after plating, and total RNA was isolated from each sample on day 8 of the experiment. After labeling, C17.2 NSCs were transferred to basal culture medium that was refreshed every 2 days. A duplicate time course experiment was performed in each series. Unlabeled C17.2 NSCs (no incubation with either SPIO/PLL or PLL) were included as a baseline reference.

Total RNA Isolation and Microarray Assay

Total RNA was extracted from C17.2 NSCs using TRI reagent (Promega, Madison, WI) and Phase Lock Gel Heavy (Eppendorf, Westbury, NY) under RNase-free conditions. RNA was purified using the RNeasy microkit (Qiagen, Valencia, CA) and quality was assessed using an Agilent 2100 Bioanalyzer microchip (Agilent, Palo Alto, CA). Microarray assays were performed on Mouse Genome 430 2.0 cDNA arrays (Affymetrix, Santa Clara, CA). Ten micrograms of biotin-labeled and fragmented cRNA was hybridized. The microarrays were hybridized, washed, and scanned according to Affymetrix standard protocols.

Gene Expression Analysis

The RNA samples were analyzed with Affymetrix Gene-Chip® Mouse Genome 430 2.0 Arrays containing 45,101 probes for over 39,000 transcripts, including 34,000 well-characterized mouse genes. Quality of the microarray experiment was assessed with *affyPLM* and *Affy*, two Bioconductor packages for statistical analysis of microarray data. To estimate the gene expression signals, data analysis was conducted on the chips' CEL file probe signal values at the Affymetrix probe pair (perfect match probe and mismatch probe) level, using the statistical algorithm robust multiarray expression measure (20) with *Affy*. This probe-level data processing includes a normalization procedure utilizing quantile normalization method (21) to reduce variation between microarrays, which might be introduced during the processes of sample preparation, manufacture, fluorescence labeling, hybridization and/or scanning. With the signal estimates, multidimensional scaling analysis was performed in *R* to assess sample variability and identified a batch effect attributed to the operation time. The expression signals were adjusted for the batch effect with the R package ComBat, using the nonparametric empiric Bayes method (http://statistics.byu.edu/johnson/ComBat/; (22)).

With the signal data in a log-transformed format, differential gene expression between individual conditions was assessed by statistical linear model analysis using the bioconductor package limma, in which an empiric Bayes method is used to moderate the standard errors of the estimated log-fold changes of gene expression and results in more stable inference and improved power, especially for experiments with small numbers of microarrays (23). Likewise, the raw *P* values provided a way to rank genes in terms of the evidence for differential gene expression in order to obtain the most likely differentially expressed genes between conditions. Analyses other than the time course analysis and pattern recognition were performed under *R* environment (http://www.r-project.org) (4).

Time course analyses were made with the software package EDGE (http://faculty.washington.edu/jstorey/edge/about.php) to identify gene expression changes over the temporal development course of day 0 through day 7 within and between the two treatment conditions PLL and SPIO/PLL. Specifically, gene expression curves over time were modeled flexibly on a natural cubic *spline* basis, and statistical significance was

calculated while accounting for sources of dependence over time (24). The raw *P* values provided a way to rank genes in terms of the evidence for differential gene expression in order to obtain the most likely differentially expressed genes over the time course. For pattern visualization, the expression data of the top ranked differentially expressed genes were scaled by the median value within each treatment condition in a per-probe manner and displayed in Heatmap, using the software package, Gene-Spring GX 7.3 (http://www.chem.agilent.com/scripts/pds.asp?lpage=27881).

The TIBCO Spotfire software was used for data visualization and organization postanalysis.

Quantitative Real-Time PCR

Real time-PCR (RT-PCR) (iScript One-Step RT-PCR; Bio-Rad) was performed to confirm the validity of the micro-array results. The relative expression of the target genes *Rnf138* and *Abcc4* in C17.2 NSCs was determined. The criteria for choosing *Rnf138* and *Abcc4* for additional verification were based on the representation of affected gene groups. The iCycler iQ Thermocycler system (Bio-Rad) was used with a lower detection limit of 1 pg of total RNA input. Total RNA (1 μL; 100 ngμL) was reverse transcribed and primers internal to the microarray probe features for *Rnf138* and *Abcc4* were used for cDNA amplification. Primer pairs were validated by analyzing PCR amplimers on a 1% agarose gel to confirm the presence of a single band of the predicted size under ultraviolet light (ethidium bromide DNA staining). In addition, melting curves were generated using the iCycler analysis software to determine whether there were any spurious amplification products. To ensure equal input conditions, RT-PCR for *ActB* (β-actin), a reference gene, was performed in parallel for each sample. After normalizing for primer amplification efficiency, raw concentrations of *Rnf138* and *Abcc4* amplimers were determined relative to *ActB* content within each sample, and statistical differences between the means (± standard deviation) untreated, PLL-treated, and SPIO/PLL-labeled samples were computed using the Student's *t* test. Data were considered statistically significant when $P < 0.05$.

RESULTS

Single-Time-Point Analysis of Individual Gene Expression

Bland-Altman plots were used to display the fold-difference (log2 SPIO/PLL minus log2 PLL) in individual gene expression versus the mean signal intensity at each time point; this approach highlights transcripts that are transiently altered following cell labeling. For example, the expression of some gene transcripts could be altered in immediate response to SPIO/PLL labeling, whereas other gene transcripts may show differences following the withdrawal of SPIO/PLL. Overall, the majority of genes (99%) expressed by C17.2 NSCs exhibited less than a 2-fold difference (log2 fold change less than ±1) in gene expression following SPIO/PLL labeling (Fig. 1). Importantly, these included genes encoding for members of the programmed cell death pathway, neural differentiation, and genes regulating cellular metabolism. Differences in gene expression outside the 2-fold threshold were considered most likely to be representative of biologically relevant gene responses to SPIO labeling. A total of 49 transcripts were differentially expressed by greater than 2-fold (log2 fold change greater than ±1) at any given point during the study, with more than half represented on day 4 after labeling (Table 1).

Several genes responsible for iron homeostasis were differentially expressed in response to SPIO/PLL labeling. Under conditions where intracellular iron is high, iron-binding proteins bind to iron responsive elements and thus regulate messenger RNA (mRNA) stability and translational activity of *Tfrc* and *FtH*, respectively. Accordingly, transferrin receptor 1 expression was strongly reduced 24–48 h after SPIO/PLL labeling (−2.25-fold) and

exhibited a gradual recovery in expression over the time course (Table 1). Similarly, the expression of ferritin heavy chain was weakly upregulated on day 1 and day 2. Finally, ceruloplasmin (also called ferroxidase) expression was strongly elevated on day 4 and day 7 after SPIO/PLL labeling. Other genes encoding for proteins important for iron homeostasis, such as aconitase 1 and aconitase 2 (*Aco1* and *Aco2*), transferrin (*Tfr*), and the transferrin receptor isoform 2 (*Tfr2*) were not affected by SPIO/PLL labeling (Fig. 1). The expression of *Aco1* and *Aco2* is weakly regulated by binding of IRPs to iron responsive elements in the 5′ untranslated region and both *Trf2* and *Tfr* lack iron responsive elements (25). Overall, the pattern of expression exhibited by genes involved in iron regulation indicates that cytosolic iron is elevated following SPIO/PLL labeling and that the activity of IRPs at genes containing iron responsive elements may be increased. These array data corroborate a previous report that applied PCR and immunoblotting detect a decrease in Trfc and an increase in Fth1 in human MSCs and human ESCs that were labeled with SPIO (14).

Rather than characterizing genes independently, microarray analysis probes the expression pattern of 39,000 transcripts, providing a broad, unbiased overview of the genetic response to treatment (e.g., SPIO/PLL labeling) at a given point in time. Other than genes directly related to iron metabolism, genes exhibiting greater than a 2-fold change in expression can be functionally grouped into lipid binding (*Fabp4*, *Lbp*), receptor signaling (*Adcy7*, *Angptl4*, *Calm3*, *Cxcl12*, *Pthlh*, *Sema5a*, *Sdf2l1*, *Tnfrsf9*, *Vegfc*), and cell stress (*Clu*, *Cp*, *Gstm2*, *Hmox1*, *Mgst1*, *Sluf1*, *Tnfrsf9*) categories. Among these, clusterin (2.93-fold), ceruloplasmin (3.01-fold), sulfatase 1 (3.90-fold), and tetraspanin 13 (3.99-fold) were the most strongly upregulated genes. Fatty acid binding protein 4 (*Fabp4*) was the most strongly downregulated (−3.39-fold) gene (Table 1).

Time Course of Differential Gene Expression Profiles

Raw *P* values from false discovery rate calculations were used to rank genes in order to obtain the most likely differentially expressed genes over the 1-week time course. Of such ranked genes exhibiting the greatest difference in expression between SPIO/PLL and PLL conditions, 2695 probe sets, representing 1399 genes, were selected for further analysis. Gene ontology analysis was performed in order to determine whether the 1399 differentially expressed genes were enriched for genes related to specific cell properties (e.g., iron binding, oxidative stress, apoptosis). Gene ontology analysis segregates genes into two major categories: (1) molecular functions of the cell and (2) biologic processes. Genes within these two categories are further parsed into gene families with related function, and the probability that a particular gene family is enriched is determined. As genes often encode for proteins that subserve multiple cellular functions, a given gene may be represented within multiple categories.

In the group of genes regulating molecular functions of the cell (1309 genes), which describe activities such as catalytic reactions or binding that occur at the molecular level, 1001 genes are involved in catalytic activity ($P = 0.000274$), structural molecule activity ($P = 0.0147$), and transcription regulator activity ($P = 0.000332$) and binding ($P = 1.95e\text{-}14$), with the largest subpopulation of genes (196, $P = 0.00195$) coding for genes involved in zinc ion binding, with a large subpopulation of genes coding for ring finger proteins.

In the group of genes involved in biologic processes, series of events accomplished by one or more ordered assemblies of molecular functions (1198 genes from the group of chosen 2695 probe sets), based on a *P* value below 0.05 (the *P* value describes the significance level in the sense that the annotations do not occur by chance), 299 genes encode regulate gene expression ($P = 1.5e\text{-}8$), as well as cellular (970 genes, $P = 0.0138$), developmental (312 genes, $P = 3.73e\text{-}5$), and metabolic (685 genes, $P = 1.36e\text{-}12$) processes and biologic regulation (431 genes, $P = 1.01e\text{-}8$). The other groups of genes affected differently by SPIO/

PLL than by PLL alone belonging to biologic processes and representing $P \leq 0.05$, are secretion, transport, locomotion, reproductive processes, and establishment of localization.

Cluster Analysis of Gene Expression Profiles

Clustering algorithms sort different objects into groups such that the degree of association between two objects is maximal if they belong to the same group (e.g., genes with similar patterns of expression over time) and minimal otherwise. Cluster analysis simply discovers structures/ relationships in data without explaining their biologic relevance. For each time point, there are three possibilities for gene expression: increased, decreased, or unchanged. Therefore, for the four time points in this study, there is a total of 81 (e.g., 3^4) unique gene expression profiles across time. Applying 81 clusters for *K*-means analysis accounted for 87% of explained variance (inertia ratio) in gene expression over time (Fig. 2). *K*-means clustering was done by correlation with data centroid-based search and yielded different clusters of the greatest possible distinction for the 2695 probe sets. The 81 clusters of transcripts show unique patterns of gene expression over the 7-day time course. Figure 3 demonstrates the expression patterns of 81 unique gene clusters. A list of the transcripts of interest, chosen from the list of most differentially regulated genes between SPIO/ PLL- and PLL-treated cells, is provided in Table 2.

Iron affects genes of many different classes, but we first analyzed the genes involved in iron metabolism. A pronounced difference between SPIO/PLL and PLL treatments was observed for the transferrin receptor (*Tfrc*), where six probes representing this gene were assigned to cluster number 76, showing pronounced downregulation of *Tfrc* in SPIO/PLL-labeled cells in comparison to PLL (Fig. 3). In contrast, other genes encoding involved in iron-dependent regulation of iron metabolism, like genes for ferritin and ferroportin/Ireg1, were not classified to the group of 1399 genes.

Iron overload can also impact a number of genes associated with metabolism and energy production. For example, NADH: dehydrogenase (ubiquinone) 1 beta subcomplex, 9 (*Ndufb9*, cluster 46), NADH: dehydrogenase (ubiquinone) Fe-S protein *7* (*Ndufs7*, cluster 51), and NADH: dehydrogenase (ubiquinone) 1 alpha subcomplex, 12 (*Ndufa12*, cluster 61) are three genes that compose the NADH ubiquinone oxidoreductase complex and contain iron in their structure. Moreover, many genes encoding for cytochromes b, c, and P450 were also affected in a different temporal pattern by SPIO/PLL treatment rather than by PLL treatment alone.

Since the present experiment was performed on neural progenitors, it is critical to evaluate the impact of SPIO/ PLL on neural genes. The time-course group of 1399 contains few genes that were affected distinctly by SPIO/ PLL labeling relative to PLL. These genes include neuronal PAS domain protein 3 (*Npas3*, cluster 7), a factor that is involved in regulation of neurogenesis, dopamine beta hydroxylase (*Dbh*, cluster 41), which encodes for protein converting norepinephrine from dopamine, and dopamine receptor 3 (*Drd3*, cluster 33). SPIO/PLL had also unique impact on LIM homeobox proteins: *Lhx1*, (cluster 33), *Lhx2*, (cluster 66) and *Lhx9* (clusters 40 and 70), which are transcriptional regulators of neuronal differentiation. Finally, another gene related to neural cells was amyloid beta (A4) precursor protein binding, family A, member 1 (*Apba1*, cluster 46), which encodes for neuronal adaptor protein that interacts with the Alzheimer's disease amyloid precursor protein. It stabilizes amyloid precursor protein and inhibits production of proteolytic amyloid precursor protein fragments, including the A beta peptide that is deposited in the brains of Alzheimer's disease patients.

Labeling with SPIO/PLL also appeared to have a significant impact on the expression of several genes that encode for ATP binding cassette proteins, two of which belong to

subfamily C (CFTR/MRP) (*Abcc*), one to subfamily D (ALD), and one to subfamily F (GCN20). Member 4 of subfamily C (*Abcc4*) and member 1 of subfamily F (*Abcf1*) were ordered to cluster 51, whereas member 5 of subfamily C (*Abcc5*) was assigned to cluster 57, and member 2 of subfamily D (*Abcd2*), to cluster 65. Finally, several genes encoding ribosomal proteins and proteins involved in ubiquitination, a process of protein delivery to the proteasome for degradation, were also altered in response to SPIO/PLL labeling. These genes, along with their ordered clusters, are indicated in Table 2. Of interest, phosphorylation of ribosomal protein S6 closely corresponds to transferrin uptake, probably under the control of the PtdIns(3,4,5)P3-mTOR signaling pathway (26), and several ribosomal proteins are known to contain iron in their structures in the form of iron-sulfur clusters.

Validation of Microarray Analyses Using Quantitative Real-Time RT-PCR

To confirm the time course and single-time-point analyses, *Rnf138* and *Abcc4* were chosen for further characterization using quantitative real-time RT-PCR. Both of these genes are present within the 2695 differentially expressed genes ranked according to false discovery rate. Rnf138, also known as NARF (Nemo-like kinase associated ring finger), is an E3 ubiquitin-protein ligase that contains a conserved N-terminal C3HC4 (Cys3-His-Cys4) RING domain that functions to coordinate two zinc ions (5,27). RING domains are found in a variety of functionally distinct proteins known to be involved in protein-DNA and protein-protein interactions. Because gene expression of RING domain family members was similarly regulated over the time course of SPIO/PLL treatment, we considered that free iron might affect the DNA binding activity via competition with zinc ion. Therefore, *Rnf138* was selected for validation using real-time RT-PCR analysis. Similarly, *Abcc4* is a member of another family of coordinately regulated genes that may be relevant for active extracellular transport of iron. *Abcc4* (ATP binding cassette, subfamily C (CFTR/MRP), member 4), is a multidrug resistance–associated protein that binds and hydrolyzes ATP to drive the transport of a variety of endogenous and xenobiotic organic anions compounds, including cyclic nucleotides, conjugated steroid hormones, and eicosanoids, across the cell membrane against a diffusion gradient (28). As detected in time course and in single-time-point analyses, quantitative real-time RT-PCR revealed that both Rnf138 and Abcc4 exhibited a significant increase in gene expression in response to SPIO/PLL on day 2 postlabeling ($P < 0.05$; Figs. 4 and 5).

DISCUSSION

Cellular labeling for serial MRI studies of nonphagocytic cells is most commonly achieved by coupling negatively charged SPIO nanoparticles to a cationic transfection agent, such as PLL or protamine sulfate, through electrostatic interactions (29,30). SPIO/transfection agent complexes are then added to cell culture medium, where they are endocytosed by cells. Previous studies show that increasing amounts of iron used for cell labeling result in higher cellular concentration of this particle (18,29). These works also report that increasing intracellular iron content does not have an effect on in vitro neuronal differentiation of C17.2 cells (18). To determine the more complex effect of magnetic nanoparticle labeling on cell function, we applied microarray technology and clustering algorithms to analyze overall gene expression by C17.2 NSCs in response to either SPIO/ PLL or PLL transfection agent over a course of 1 week in vitro.

Analysis of relative fold differences in gene expression for each time point revealed that genes responsible for iron homeostasis, lysosomal function, detoxification, signal transduction, growth factors, and lipid peroxidation are differentially expressed by more than 2-fold following SPIO/PLL labeling. Relative to cells treated with PLL transfection agent, C17.2 NSCs labeled with SPIO/PLL complexes exhibited differential (either

increased or decreased) expression of genes throughout the time course from which, based on the maximum difference in gene expression between SPIO/PLL- and PLL-treated cells, the top 2695 gene probes representing 1399 genes were further analyzed. Among the 1399 genes, genes encoding zinc-binding proteins were highly enriched. In comparison, genes encoding for proteins involved in apoptosis/ programmed cell death did not reveal differences in expression.

Iron is an essential cofactor for cell proliferation, mitochondrial function, and oxygen transport (heme). However, an excess accumulation of intracellular free iron can oxidize and damage the protein, lipid, and nucleic acid components of cells. The expression of proteins important for iron transport (transferrin receptor) and iron storage (ferritin) is coordinately and reciprocally regulated at the posttranscriptional level by IRPs (IRP-1 and IRP-2), which act as sensors of cytosolic iron concentration (14). For example, when iron is abundant, IRP-1 lacks binding activity at iron-responsive elements found in the mRNA of target transcripts and IRP-2 is targeted for degradation by the ubiquitin-proteosomal system. In the absence of IRP binding, the translation of ferritin mRNA is no longer repressed and the half-life of transferrin receptor mRNA is reduced, resulting in sequestration of excess cytosolic iron within ferritin. The overall gene expression profile of C17.2 NSCs following SPIO/PLL labeling observed herein is indicative of such a cellular response to an elevation in intracellular free iron concentration.

SPIO nanoparticles consist of an iron oxide nanocrystal encased within a shell of crosslinked dextran. Following intravenous injection into the blood pool for medical diagnostic purposes, SPIO nanoparticles accumulate within the liver and spleen, where they are metabolized and molecular iron is incorporated into hemoglobin (31). Typically, between 5 and 20 pg of iron per cell, or between 50 and 200 times the normal endogenous cell level, is introduced by SPIO labeling, excluding erythrocytes, which contain ~30 pg of iron (32). However, very little is known about the intracellular fate of SPIO nanoparticles following endocytosis. It has been proposed that the acidic milieu of the lysosomal compartment (~pH 5.5) may disrupt the dextran shell and liberate Fe^{3+} from iron oxide nanoparticles (12). While mammalian cells lack dextranases, sulfatases are lysosomal enzymes that cleave a range of sulfated carbohydrates. Though it is not known whether the dextran shell of SPIO nanoparticles is sulfated by sulfotransferases within the cell, *Sulf1* expression was strongly upregulated on day 4 (3.9-fold) after SPIO/PLL labeling. As shown for cellular iron overload (33), coordinated and reciprocal changes in transferrin receptor 1 and ferritin mRNA and protein are induced following SPIO labeling (13), suggesting that the integrity of the dextran shell is compromised and cytosolic free iron is increased; this may lead to increase of reactive oxygen species. However, previous studies demonstrated that the generation of reactive oxygen species is not induced after SPIO labeling (7,13). While heme oxygenase 1 was transiently upregulated on day 1, a limited role for reactive oxygen species signaling after SPIO labeling is supported by the upregulation of ceruloplasmin expression at later time points, a protein that is responsible for the conversion of Fe^{2+} to the less oxidative form, Fe^{3+}. Also, lipid peroxidation, another metabolic pathway influenced by changes in iron level, was not affected.

Gene expression profiling of liver tissue obtained from knockout mice lacking the gene that encodes for hereditary hemochromatosis protein or *Hfe* (34), which, when mutated, is the one of the major factors precipitating iron overload (35), revealed upregulation of genes involved in antioxidant defense and downregulation of genes involved in cholesterol metabolism. In comparison, gene profiling of skeletal and heart muscle from mice fed a high-iron diet (2% carbonyl iron) for 6 weeks exhibited limited changes in the expression of genes involved in cell stress responses and lipid metabolism despite a greater than 10-fold increase in hepatic iron content (36). These studies highlight tissue specific responses to iron

overload and the capacity of certain tissues to sustain relatively normal gene expression patterns despite persistently elevated iron. Iron is particularly important for the development of oligodendrocytes in the central nervous system (37) and chronically or abnormally elevated iron is implicated in the pathogenesis of several central nervous system diseases (38). However, acute overnight exposure of C17.2 NSCs to SPIO for cell labeling appears to be well tolerated, as indicated by the early (e.g., day 1 and day 2) change in the expression of genes important for iron metabolism followed by the late (e.g., day 4 and day 7) induction of several genes essential for the control of cell stress (*Cp*, *Hmox1*, *Gstm2*).

By increasing the sampling density in microarray studies, it may be possible to further define immediate (e.g., 6 h or 12 h) and very long-term (e.g., 2 weeks and beyond) cellular responses to SPIO/PLL labeling. The time points selected for this study provide an optimal overview of the genomic response of C17.2 NSCs to SPIO/PLL labeling for a typical cell-tracking study. Other than the early induction of a homeostatic response in iron metabolism and the late changes in cell signaling and oxidative stress pathways, the pattern of gene expression found in C17.2 NSCs after overnight exposure to SPIO/PLL is highly similar to that of C17.2 NSC treated with PLL. The observed changes were not very pronounced, specifically, genes encoding for factors regulating programmed cell death, oxidative stress, neuronal cell function, and cell metabolism exhibited no remarkable change in expression, with few exceptions. In previous studies, it was shown that deferoxamine, an effective iron chelator, causes a decrease in expression of few mitochondrial genes involved in metabolism, between them NADH: ubiquinone oxidoreductase, known as complex 1 of respiratory electron transport chain (39). Though it is not known whether the effects of iron chelators are attributable to iron removal from target proteins or to indirect effects on intracellular iron stores, the present study revealed that *Ndufs7*, *Ndufa12*, and *Ndufb9*, each of which are parts of NADH ubiquinone oxidoreductase that contain iron in their structure, were differently affected in cells labeled with SPIO/PLL in comparison to treatment with PLL transfection agent. Also, a recent report about increased expression of *Abcc4* in the presence of high iron accumulation in the cells of *hfe* −/− mice (40) is consistent with the results of SPIO/PLL NSC labeling.

Taken together, the genes that were differentially expressed in response to SPIO/PLL are indicative of a coordinated early homeostatic cellular response to increased intracellular iron concentration. However, while common themes are emerging from independent studies of cellular responses to acute (e.g., cell labeling) and chronic (e.g., genetic deficiency or dietary excess) iron overload, it is important to emphasize that the pattern of gene expression by C17.2 NSC in response to SPIO/PLL may differ from that of other cell types. Overall, intracellular labeling using SPIO/PLL in preparation for MR cell tracking studies poses no obvious adverse effects on cell viability, function, and gene expression, indicating that initiating clinical studies appears to be justified (5).

Acknowledgments

The C17.2 NSC line was obtained as a courtesy of Drs. E. Y. Snyder and J. H. Wolfe. The authors thank C. Connover Talbot Jr. (JHMI Microarray Core Facility) and Dr. Joe Nielsen (LDN, NINDS, National Institutes of Health) for assisting with analysis of gene expression data. We also thank Dr. Gregg Semenza (Vascular Biology Program, ICE, JHSOM) for allowing access to their Bio-Rad iCycler. This study was supported by 2RO1 NS045062 and NMSS RG3630. Dr. Jeff Bulte is a paid consultant for Surgivision Inc., a medical device company. This arrangement has been approved by The Johns Hopkins University in accordance with its Conflict of Interest policies.

References

1. Ferrucci JT, Stark DD. Iron oxide-enhanced MR imaging of the liver and spleen: review of the first 5 years. AJR Am J Roentgenol 1990;155:943–950. [PubMed: 2120963]

2. de Vries IJ, Lesterhuis WJ, Barentsz JO, Verdijk P, van Krieken JH, Boerman OC, Oyen WJ, Bonenkamp JJ, Boezeman JB, Adema GJ, Bulte JW, Scheenen TW, Punt CJ, Heerschap A, Figdor CG. Magnetic resonance tracking of dendritic cells in melanoma patients for monitoring of cellular therapy. Nat Biotechnol 2005;23:1407–1413. [PubMed: 16258544]
3. Zhu JZ, XingWu LF. Tracking neural stem cells in patients with brain trauma. N Engl J Med 2006;355:2376–2378. [PubMed: 17135597]
4. Toso C, Vallee JP, Morel P, Ris F, Demuylder-Mischler S, Lepetit-Coiffe M, Marangon N, Saudek F, James Shapiro AM, Bosco D, Berney T. Clinical magnetic resonance imaging of pancreatic islet grafts after iron nanoparticle labeling. Am J Transplant 2008;8:701–706. [PubMed: 18294167]
5. Bulte JW. In vivo MRI cell tracking: clinical studies. AJR Am J Roentgenol 2009;193:314–325. [PubMed: 19620426]
6. Bulte JW, Douglas T, Witwer B, Zhang SC, Strable E, Lewis BK, Zywicke H, Miller B, van Gelderen P, Moskowitz BM, Duncan ID, Frank JA. Magnetodendrimers allow endosomal magnetic labeling and in vivo tracking of stem cells. Nat Biotechnol 2001;19:1141–1147. [PubMed: 11731783]
7. Arbab AS, Bashaw LA, Miller BR, Jordan EK, Lewis BK, Kalish H, Frank JA. Characterization of biophysical and metabolic properties of cells labeled with superparamagnetic iron oxide nanoparticles and transfection agent for cellular MR imaging. Radiology 2003;229:838–846. [PubMed: 14657318]
8. Kostura L, Kraitchman DL, Mackay AM, Pittenger MF, Bulte JW. Feridex labeling of mesenchymal stem cells inhibits chondrogenesis but not adipogenesis or osteogenesis. NMR Biomed 2004;17:513–517. [PubMed: 15526348]
9. Bulte JW, Kraitchman DL. Iron oxide MR contrast agents for molecular and cellular imaging. NMR Biomed 2004;17:484–499. [PubMed: 15526347]
10. Henning TD, Sutton EJ, Kim A, Golovko D, Horvai A, Ackerman L, Sennino B, McDonald D, Lotz J, Daldrup-Link HE. The influence of ferucarbotran on the chondrogenesis of human mesenchymal stem cells. Contrast Media Mol Imaging 2009;4:165–173. [PubMed: 19670250]
11. Siglienti I, Bendszus M, Kleinschnitz C, Stoll G. Cytokine profile of iron-laden macrophages: implications for cellular magnetic resonance imaging. J Neuroimmunol 2006;173:166–173. [PubMed: 16380168]
12. Arbab AS, Wilson LB, Ashari P, Jordan EK, Lewis BK, Frank JA. A model of lysosomal metabolism of dextran coated superparamagnetic iron oxide (SPIO) nanoparticles: implications for cellular magnetic resonance imaging. NMR Biomed 2005;18:383–389. [PubMed: 16013087]
13. Pawelczyk E, Arbab AS, Pandit S, Hu E, Frank JA. Expression of transferrin receptor and ferritin following ferumoxides-protamine sulfate labeling of cells: implications for cellular magnetic resonance imaging. NMR Biomed 2006;19:581–592. [PubMed: 16673357]
14. Rouault TA. The role of iron regulatory proteins in mammalian iron homeostasis and disease. Nat Chem Biol 2006;2:406–414. [PubMed: 16850017]
15. Templeton DM, Liu Y. Genetic regulation of cell function in response to iron overload or chelation. Biochim Biophys Acta 2003;1619:113–124. [PubMed: 12527106]
16. Brown AB, Yang W, Schmidt NO, Carroll R, Leishear KK, Rainov NG, Black PM, Breakefield XO, Aboody KS. Intravascular delivery of neural stem cell lines to target intracranial and extracranial tumors of neural and non-neural origin. Hum Gene Ther 2003;14:1777–1785. [PubMed: 14670128]
17. Heine W, Conant K, Griffin JW, Hoke A. Transplanted neural stem cells promote axonal regeneration through chronically denervated peripheral nerves. Exp Neurol 2004;189:231–240. [PubMed: 15380475]
18. Magnitsky S, Walton RM, Wolfe JH, Poptani H. Magnetic resonance imaging detects differences in migration between primary and immortalized neural stem cells. Acad Radiol 2008;15:1269–1281. [PubMed: 18790399]
19. Walczak P, Kedziorek DA, Gilad AA, Barnett BP, Bulte JW. Applicability and limitations of MR tracking of neural stem cells with asymmetric cell division and rapid turnover: the case of the shiverer dysmyelinated mouse brain. Magn Reson Med 2007;58:261–269. [PubMed: 17654572]

20. Irizarry RA, Hobbs B, Collin F, Beazer-Barclay YD, Antonellis KJ, Scherf U, Speed TP. Exploration, normalization, and summaries of high density oligonucleotide array probe level data. Biostatistics 2003;4:249–264. [PubMed: 12925520]
21. Bolstad BM, Irizarry RA, Astrand M, Speed TP. A comparison of normalization methods for high density oligonucleotide array data based on variance and bias. Bioinformatics 2003;19:185–193. [PubMed: 12538238]
22. Johnson WE, Li C, Rabinovic A. Adjusting batch effects in microarray expression data using empirical Bayes methods. Biostatistics 2007;8:118–127. [PubMed: 16632515]
23. Smith J, Speed D, Hocking PM, Talbot RT, Degen WG, Schijns VE, Glass EJ, Burt DW. Development of a chicken 5 K microarray targeted towards immune function. BMC Genomics 2006;7:49. [PubMed: 16533398]
24. Storey JD, Akey JM, Kruglyak L. Multiple locus linkage analysis of genomewide expression in yeast. PLoS Biol 2005;3:e267. [PubMed: 16035920]
25. Kawabata H, Germain RS, Ikezoe T, Tong X, Green EM, Gombart AF, Koeffler HP. Regulation of expression of murine transferrin receptor 2. Blood 2001;98:1949–1954. [PubMed: 11535534]
26. Galvez T, Teruel MN, Heo WD, Jones JT, Kim ML, Liou J, Myers JW, Meyer T. siRNA screen of the human signaling proteome identifies the PtdIns(3,4,5)P3-mTOR signaling pathway as a primary regulator of transferrin uptake. Genome Biol 2007;8:R142. [PubMed: 17640392]
27. Giannini AL, Gao Y, Bijlmakers MJ. T-cell regulator RNF125/TRAC-1 belongs to a novel family of ubiquitin ligases with zinc fingers and a ubiquitin-binding domain. Biochem J 2008;410:101–111. [PubMed: 17990982]
28. Russel FG, Koenderink JB, Masereeuw R. Multidrug resistance protein 4 (MRP4/ABCC4): a versatile efflux transporter for drugs and signalling molecules. Trends Pharmacol Sci 2008;29:200–207. [PubMed: 18353444]
29. Frank JA, Zywicke H, Jordan EK, Mitchell J, Lewis BK, Miller B, Bryant LH Jr, Bulte JW. Magnetic intracellular labeling of mammalian cells by combining (FDA-approved) superparamagnetic iron oxide MR contrast agents and commonly used transfection agents. Acad Radiol 2002;9(suppl 2):S484–487. [PubMed: 12188316]
30. Kalish H, Arbab AS, Miller BR, Lewis BK, Zywicke HA, Bulte JW, Bryant LH Jr, Frank JA. Combination of transfection agents and magnetic resonance contrast agents for cellular imaging: relationship between relaxivities, electrostatic forces, and chemical composition. Magn Reson Med 2003;50:275–282. [PubMed: 12876703]
31. Weissleder R, Stark DD, Engelstad BL, Bacon BR, Compton CC, White DL, Jacobs P, Lewis J. Superparamagnetic iron oxide: pharmacokinetics and toxicity. AJR Am J Roentgenol 1989;152:167–173. [PubMed: 2783272]
32. Winoto-Morbach S, Tchikov V, Muller-Ruchholtz W. Magnetophoresis, II: quantification of iron and hemoglobin content at the single erythrocyte level. J Clin Lab Anal 1995;9:42–46. [PubMed: 7722771]
33. Zahringer J, Baliga BS, Munro HN. Novel mechanism for translational control in regulation of ferritin synthesis by iron. Proc Natl Acad Sci U|S|A 1976;73:857–861.
34. Coppin H, Darnaud V, Kautz L, Meynard D, Aubry M, Mosser J, Martinez M, Roth MP. Gene expression profiling of Hfe−/− liver and duodenum in mouse strains with differing susceptibilities to iron loading: identification of transcriptional regulatory targets of Hfe and potential hemochromatosis modifiers. Genome Biol 2007;8:R221. [PubMed: 17945001]
35. Feder JN, Gnirke A, Thomas W, Tsuchihashi Z, Ruddy DA, Basava A, Dormishian F, Domingo R Jr, Ellis MC, Fullan A, Hinton LM, Jones NL, Kimmel BE, Kronmal GS, Lauer P, Lee VK, Loeb DB, Mapa FA, McClelland E, Meyer NC, Mintier GA, Moeller N, Moore T, Morikang E, Prass CE, Quintana L, Starnes SM, Schatzman RC, Brunke KJ, Drayna DT, Risch NJ, Bacon BR, Wolff RK. A novel MHC class I like gene is mutated in patients with hereditary haemochromatosis. Nat Genet 1996;13:399–408. [PubMed: 8696333]
36. Rodriguez A, Hilvo M, Kytomaki L, Fleming RE, Britton RS, Bacon BR, Parkkila S. Effects of iron loading on muscle: genome-wide mRNA expression profiling in the mouse. BMC Genomics 2007;8:379. [PubMed: 17949489]

37. Roskams AJ, Connor JR. Iron, transferrin, and ferritin in the rat brain during development and aging. J Neurochem 1994;63:709–716. [PubMed: 8035195]

38. Jeong SY, Rathore KI, Schulz K, Ponka P, Arosio P, David S. Dysregulation of iron homeostasis in the CNS contributes to disease progression in a mouse model of amyotrophic lateral sclerosis. J Neurosci 2009;29:610–619. [PubMed: 19158288]

39. Ye Z, Connor JR. Screening of transcriptionally regulated genes following iron chelation in human astrocytoma cells. Biochem Biophys Res Commun 1999;264:709–713. [PubMed: 10543996]

40. Arch DD, Bergeron M, Hathaway L, Kushner JP, Phillips JD, Franklin MR. Longitudinal study of a mouse model of familial porphyria cutanea tarda. Cell Mol Biol (Noisy-le-grand) 2009;55:46–54. [PubMed: 19656451]

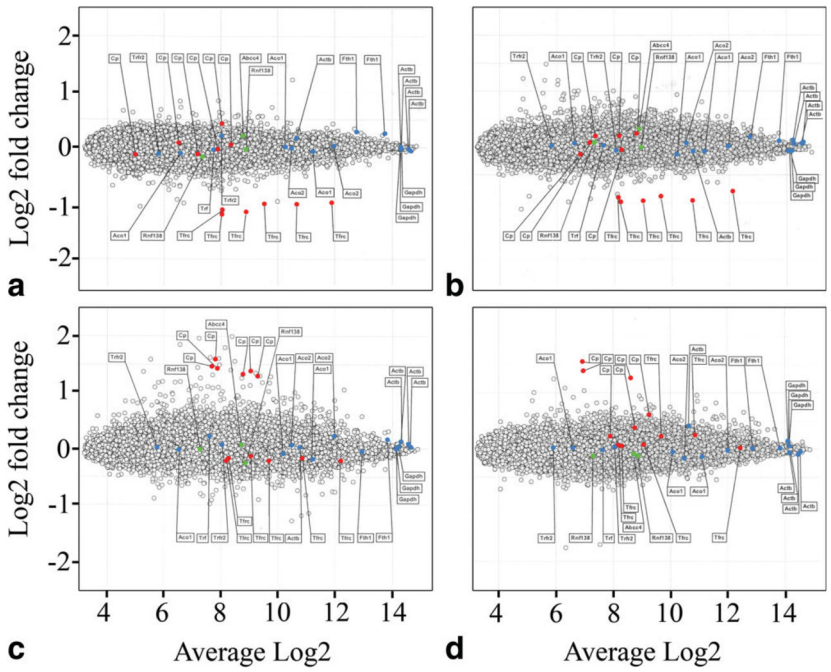

FIG. 1.

Bland-Altman plots of the log2 fold change in gene expression versus mean expression of each gene at single time points. Probes for reference genes (blue filled circles, *Actb*, *Aco1*, *Aco2*, *Fth1*, *Gapdh*, *Trf*, *Trfr2*) and genes of interest (green filled circles, *Abcc4*, *Rnf138*), and iron metabolism genes exhibiting greater than a 2-fold change in expression in at least one particular time point (red filled circles, *Cp*, *Trfc*) in C17.2 NSCs are highlighted on day 1 **(a)**, day 2 **(b)**, day 4 **(c)**, and day 7 **(d)** after SPIO/PLL labeling. Probes for genes exhibiting less than a 2-fold difference in expression are represented by gray filled circles. Several genes (e.g., *Actb*, *Cp*, *Fth1*, *Gapdh*, *Tfrc*) are represented by hybridization signal from multiple probes, distributed along the 5′ to 3′ extent of each transcript, indicating the quality of the RNA isolation and hybridization process. Raw fold change values are indicated in Table 1.

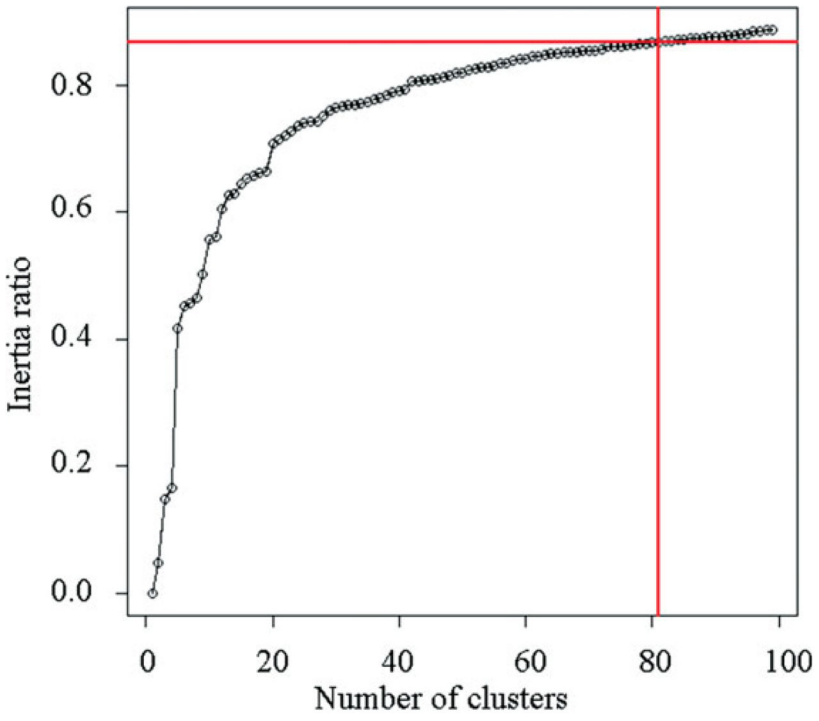

FIG. 2.
Graph demonstrating 81 clusters explaining 87% of the explained variance (inertia ratio). [Color figure can be viewed in the online issue, which is available at www.interscience.wiley.com.]

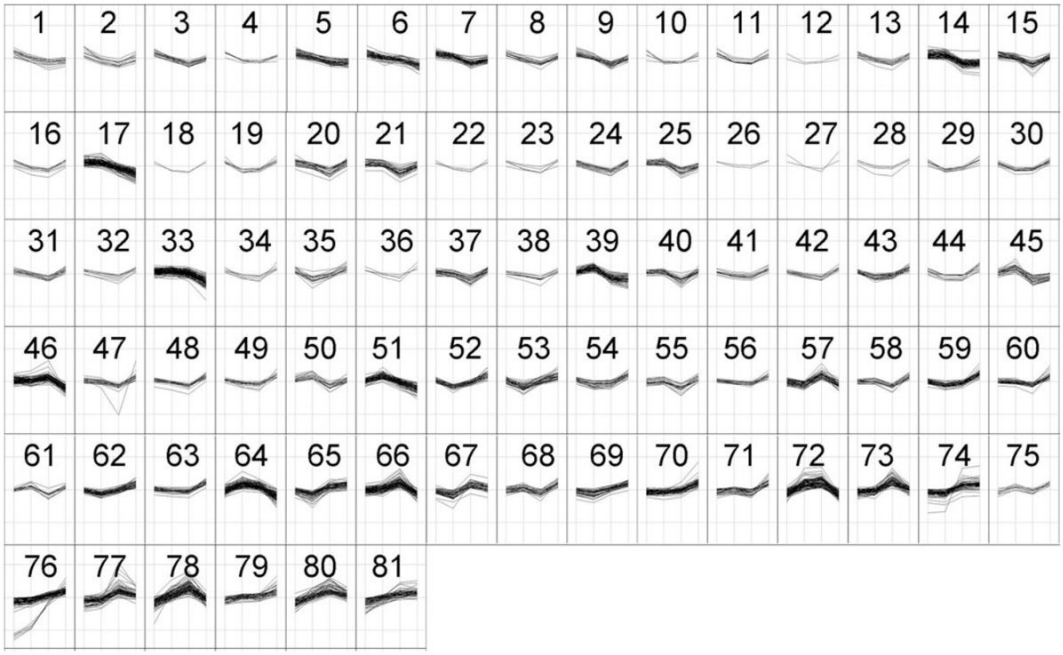

FIG. 3.

K-means clustering of 2695 gene probes assembled into 81 clusters for SPIO/PLL relative to PLL labeling, illustrated in log2 scale of fold change with blinded dimensions to conditioning variables. Genes exhibiting potentially important expression profiles over time are indicated in Table 2.

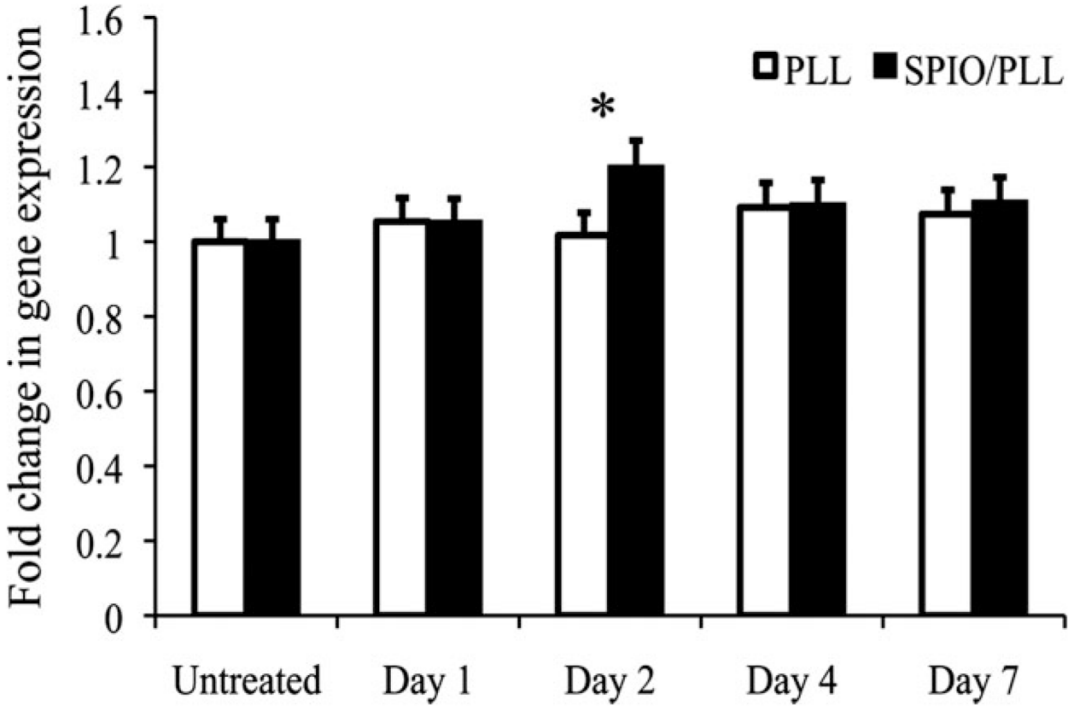

FIG. 4.

Quantitative real-time RT-PCR analysis of Rnf138 mRNA expression in C17.2 NSCs. The expression of Rnf138 mRNA in PLL-treated versus SPIO/PLL-labeled C17.2 NSCs was analyzed using mRNA from samples isolated over the time course of the microarray study. The result values are expressed as the mean of quadruplicate real-time RT-PCR assays. Error bars denote standard deviations. After normalizing for β-actin mRNA content, statistically significant differences between untreated, PLL-treated, and SLIO/PLL-labeled C17.2 NSC were determined. *$P < 0.05$.

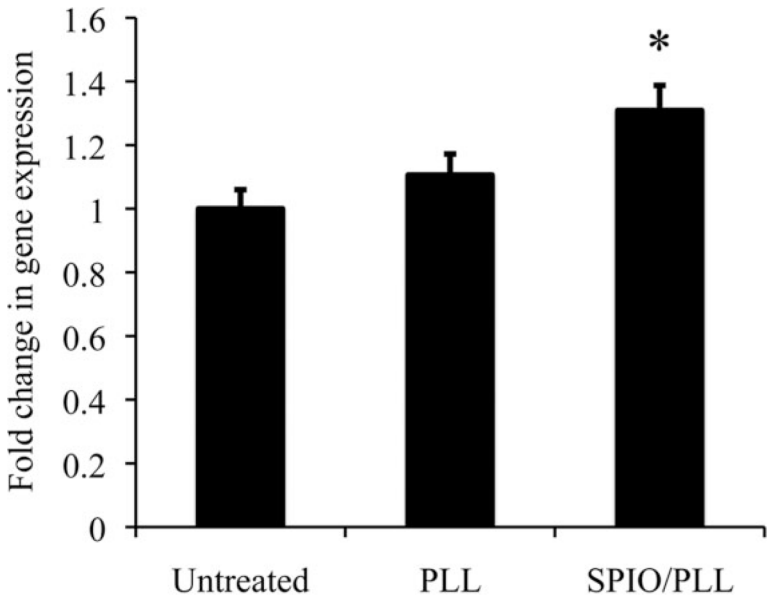

FIG. 5.

Quantitative real-time RT-PCR analysis of Abcc4 mRNA expression in C17.2 NSCs. The expression of Abcc4 mRNA in PLL-treated versus SPIO/PLL-labeled C17.2 NSCs was analyzed using mRNA from samples isolated on day 2 of the microarray study. The result values are expressed as the mean of quadruplicate real-time RT-PCR assays. Error bars denote standard deviations. After normalizing for β-actin mRNA content, statistically significant differences between untreated, PLL-treated, and SLIO/ PLL-labeled C17.2 NSC were determined. *$P < 0.05$.

Magn Reson Med. Author manuscript; available in PMC 2010 April 22.

Table 1

List of Genes That Were Differentially Expressed by More Than 2-Fold in C17.2 NSCs at Any Measured Time Point After SPIO/PLL Labeling*

		Day					
Gene symbol	**Gene title**	**1**	**2**	**4**	**7**	**Accession**	**Probe name**
Adcy7	adenylate cyclase 7	−1.25	−1.04	2.06	1.21	NM_007406	1450065_at
Adcy7	adenylate cyclase 7	−1.09	−1.07	2.14	1.20	BB746807	1456307_s_at
Angptl4	angiopoietin-like 4	−1.09	1.13	2.18	−1.01	NM_020581	1417130_s_at
Btc	betacellulin, epidermal growth factor family member	−2.00	−1.65	− 1.55	−1.10	NM_007568	1421161_at
C1r	complement component 1, r subcomponent	1.27	1.13	2.09	1.28	NM_023143	1417009_at
C1s	complement component 1, s subcomponent	1.09	−1.21	2.26	1.30	BC022123	1424041_s_at
Calm3	Calmodulin 3	−2.08	1.09	1.02	−1.15	AV047570	1438825_at
Cd24a	CD24a antigen	−1.03	2.28	1.32	1.33	NM_009846	1416034_at
Clu	clusterin	1.16	1.14	2.93	1.19	NM_013492	1418626_a_at
Clu	clusterin	−1.08	1.09	2.53	1.14	AV152288	1437689_x_at
Clu	clusterin	1.14	1.00	2.43	1.17	BB433678	1454849_x_at
Col12a1	collagen, type XII, alpha 1	−1.28	1.07	2.48	1.00	BB114398	1434411_at
Col1a1	collagen, type I, alpha 1	−1.23	−1.11	2.07	1.10	U08020	1423669_at
Colec12	collectin sub-family member 12	−1.13	1.80	2.72	1.15	NM_130449	1419693_at
Cp	ceruloplasmin	1.04	1.19	2.45	1.52	BB332449	1417494_a_at
Cp	ceruloplasmin	1.35	−1.04	2.60	2.40	BB332449	1417495_x_at
Cp	ceruloplasmin	−1.07	1.15	3.01	2.93	BB332449	1417496_at
Cp	ceruloplasmin	1.06	−1.09	2.77	2.62	BB332449	1448734_at
Cp	ceruloplasmin	−1.10	1.06	2.70	1.18	BB332449	1448735_at
Cp	ceruloplasmin	−1.01	1.15	2.49	1.29	BB009037	1455393_at
Creld2	cysteine-rich with EGF-like domains 2	−1.01	−1.54	− 2.44	−1.12	AK017880	1452754_at
Ctgf	connective tissue growth factor	−1.02	1.37	2.28	−1.35	NM_010217	1416953_at
Cxcl12	chemokine (C-X-C motif) ligand 12	−1.11	2.01	1.90	1.09	BC006640	1448823_at
Dcn	decorin	1.18	1.09	2.39	−1.11	NM_007833	1449368_at
Dpt	dermatopontin	1.11	1.31	2.81	1.17	NM_019759	1418511_at
Evi2a	ecotropic viral integration site 2a	−1.05	1.33	2.14	1.26	NM_010161	1450241_a_at
Fabp4	fatty acid binding protein 4, adipocyte	1.26	−1.97	− 1.04	−3.25	NM_024406	1417023_a_at

Gene symbol	Gene title	Day 1	Day 2	Day 4	Day 7	Accession	Probe name
Fabp4	fatty acid binding protein 4, adipocyte	1.04	−2.16	− 1.04	−3.39	BC002148	1451263_a_at
Fn1	fibronectin 1	−1.10	1.04	2.12	−1.03	BM234360	1437218_at
Fstl1	follistatin-like 1	−1.20	1.28	2.24	1.22	BI452727	1416221_at
Fstl1	follistatin-like 1	−1.19	1.21	2.25	1.22	BI452727	1448259_at
Gstm2	glutathione S-transferase, mu 2	1.22	1.21	1.38	2.05	NM_008183	1416411_at
Hmox1	heme oxygenase (decycling) 1	2.32	−1.16	− 1.25	1.10	NM_010442	1448239_at
Hs6st2	heparan sulfate 6-O-sulfotransferase 2	−1.12	1.01	2.28	−1.04	AW536432	1450047_at
Lbp	lipopolysaccharide binding protein	1.16	1.14	3.04	1.42	NM_008489	1448550_at
LOC640441///Thbs1	similar to thrombospondin 1///thrombospondin 1	−1.45	2.29	1.98	1.01	AI385532	1421811_at
Lrrc17	leucine rich repeat containing 17	−1.15	−1.46	2.02	1.23	BB503935	1429679_at
Mgp	matrix Gla protein	−1.11	−1.06	3.08	−1.13	NM_008597	1448416_at
Mgst1	microsomal glutathione S-transferase 1	1.01	1.93	2.39	1.38	BI150149	1415897_a_at
Mme	membrane metallo endopeptidase	1.04	−1.11	2.15	1.70	NM_008604	1422975_at
Mrc2	mannose receptor, C type 2	1.01	1.44	2.63	1.33	BB528408	1421045_at
Myadm	myeloid-associated differentiation marker	1.01	−1.32	2.18	−1.46	BB500055	1439389_s_at
Pdgfb	platelet derived growth factor, B polypeptide	−1.02	2.00	1.30	1.18	BC023427	1450414_at
Pdia4	protein disulfide isomerase associated 4	−1.14	−1.10	−2.22	1.29	J05186	1416497_at
Pthlh	parathyroid hormone-like peptide	−1.14	2.33	2.26	1.39	NM_008970	1422324_a_at
Robo1	roundabout homolog 1 (Drosophila)	1.07	1.01	3.00	1.25	BG065230	1427231_at
Sdf2l1	stromal cell-derived factor 2-like 1	−1.08	−1.28	−2.28	1.01	NM_022324	1418206_at
Sema5a	sema domain, seven thrombospondin repeats (type 1 and type 1-like), (semaphorin) 5A	−1.10	1.34	2.58	1.53	AV375653	1437422_at
Serinc3	serine incorporator 3 solute carrier family 18 (vesicular monoamine), member	−1.04	−1.11	1.26	2.00	NM_012032	1448847_at
Slc18a2	2	1.18	−1.25	1.05	2.11	AV334638	1437079_at
Steap2	six transmembrane epithelial antigen of prostate 2	−1.29	−1.31	1.50	2.36	BB529332	1446071_at
Sulf1	sulfatase 1	−1.37	1.14	3.61	1.12	BB751459	1436319_at
Sulf1	sulfatase 1	−1.30	1.20	3.90	1.51	BB065799	1438200_at
Tapbp	TAP binding protein	−1.13	1.29	2.00	1.29	AF043943	1421812_at
Tapbp	TAP binding protein	−1.22	1.53	2.03	1.31	AF043943	1450378_at
Tfrc	transferrin receptor	−2.03	−1.94	−1.11	1.21	BB810450	1422966_a_at

Gene symbol	Gene title	Day 1	Day 2	Day 4	Day 7	Accession	Probe name
Tfrc	transferrin receptor	−2.23	−1.95	−1.09	1.07	BB810450	1422967_a_at
Tfrc	transferrin receptor	−1.98	−1.72	−1.17	1.01	AK011596	1452661_at
AFFX-Tfrc	AFFX-transferrin receptor	−2.01	−1.84	−1.15	1.16	TransRecMur/X57349_3	TransRecMur/X57349_3_at
AFFX-Tfrc	AFFX-transferrin receptor	−2.25	−1.97	−1.11	1.04	TransRecMur/X57349_5	TransRecMur/X57349_5_at
AFFX-Tfrc	AFFX-transferrin receptor	−2.18	−1.86	−1.16	1.05	TransRecMur/X57349_M	TransRecMur/X57349_M_at
Tiam2	T-cell lymphoma invasion and metastasis 2	1.16	2.17	1.24	1.03	BM228957	1423186_at
Tnfrsf9	tumor necrosis factor receptor superfamily, member 9	1.12	1.03	2.13	1.81	BC028507	1428034_a_at
Trim25	tripartite motif-containing 25	1.04	2.00	1.28	−1.01	AA960166	1419879_s_at
Tspan13	tetraspanin 13	−1.33	1.16	3.99	1.24	BB807707	1418643_at
Tspan13	tetraspanin 13	−1.01	1.06	2.14	1.04	BB807707	1460239_at
Vegfc	vascular endothelial growth factor C	−1.10	2.80	1.83	1.02	BB089170	1439766_x_at

*Raw fold change values for each measured time point are indicated, along with the NCBI gene accession identifier and the Affymetrix probe name for each gene. Several genes (e.g., Adcy7, Clu, Cp, Fabp4, Fstl1, Sulf1, Tapbp, Tfrc, and Tspan13) are represented by hybridization signal from multiple microarray probes positioned along the 5′ to 3′ length of their respective RNA transcripts.

Table 2

List of Selected Genes From the Set of 2695 Probes That Exhibited the Greatest Difference in Expression (SPIO/PLL Labeling Relative to PLL Treatment) Over the 1-Week Time Course Study*

Gene symbol	Gene title	Cluster	Accession	Probe number
Tfrc	transferrin receptor	76	NM_011638	1422966_a_at
Tfrc	transferrin receptor	76	NM_011638	1422967_a_at
Tfrc	transferrin receptor	76	NM_011638	1452661_at
Tfrc	transferrin receptor	76	NM_011638	AFFX-TransRecMur/X57349_3_at
Tfrc	transferrin receptor	76	NM_011638	AFFX-TransRecMur/X57349_5_at
Tfrc	transferrin receptor	76	NM_011638	AFFX TransRecMur/X57349_M_at
Npas3	neuronal PAS domain protein 3	7	NM_013780	1450287_at
Nptx2	neuronal pentraxin 2	59	NM_016789	1420720_at
Dbh	dopamine beta hydroxylase	41	NM_138942	1447592_at
Drd3	dopamine receptor 3	33	NM_007877	1422278_at
Ldb2	LIM domain binding 2	29	NM_001077398	1421101_a_at
Limd1	LIM domains containing 1	51	NM_013860	1422731_at
Lhx1	LIM homeobox protein 1	33	NM_008498	1450428_at
Lhx2	LIM homeobox protein 2	66	NM_010710	1418317_at
Lhx9	LIM homeobox protein 9	70	NM_001025565	1419324_at
Lhx9	LIM homeobox protein 9	40	NM_001025565	1431598_a_at
Limk2	LIM motif-containing protein kinase 2	31	NM_001034030	1439896_at
Apba1	amyloid beta (A4) precursor protein binding, family A, member 1	46	NM_177034	1459605_at
Abcc4	ATP-binding cassette, sub-family C (CFTR/MRP), member 4	51	NM_001033336	1443870_at
Abcc5	ATP-binding cassette, sub-family C (CFTR/MRP), member 5	57	NM_013790	1447384_at
Abcd2	ATP-binding cassette, sub-family D (ALD), member 2	65	NM_011994	1439835_x_at
Abcf1	ATP-binding cassette, sub-family F (GCN20), member 1	51	NM_013854	1452236_at
Mrpl1	mitochondrial ribosomal protein L1	60	NM_001039084	1460508_at
Mrpl15	mitochondrial ribosomal protein L15	52	NM_025300	1460490_at
Mrpl3	mitochondrial ribosomal protein L3	17	NM_053159	1422463_a_at
Mrpl3	mitochondrial ribosomal protein L3	17	NM_053159	1422464_at
Mrpl37	mitochondrial ribosomal protein L37	51	NM_025500	1423764_s_at
Mrpl38	mitochondrial ribosomal protein L38	51	NM_024177	1447961_s_at
Mrps25	mitochondrial ribosomal protein S25	66	NM_025578	1418716_at
Mrps9	mitochondrial ribosomal protein S9	14	NM_023514	1435843_x_at
Rpl14	ribosomal protein L14	21	NM_025974	1426793_a_at
Rpl17	ribosomal protein L17	15	NM_001002239	1423855_x_at
Rpl22l1	ribosomal protein L22 like 1	55	NM_026517	1417126_a_at
Rpl27	ribosomal protein L27	14	NM_001110339	1448217_a_at
Rpl27a	ribosomal protein L27a	7	NM_011975	1426661_at
Rpl31	ribosomal protein L31	44	NM_053257	1441304_at

Gene symbol	Gene title	Cluster	Accession	Probe number
Rpl35	ribosomal protein L35	15	NM_025592	1436840_x_at
Rpl35	ribosomal protein L35	8	NM_025592	1454856_x_at
Rpl37	ribosomal protein L37	61	NM_026069	1434872_x_at
Rpl39	ribosomal protein L39	35	NM_026055	1423032_at
Rpl4	ribosomal protein L4	70	NM_024212	1425183_a_at
Rpl41	ribosomal protein L41	33	NM_018860	1446726_at
Rpl7	ribosomal protein L7	53	NM_011291	1415979_x_at
Rpl7	ribosomal protein L7	43	NM_011291	1426162_a_at
Rpl8	ribosomal protein L8	7	NM_012053	1417762_a_at
Rps12	ribosomal protein S12	41	NM_011295	1447205_x_at
Rps13	ribosomal protein S13	15	NM_026533	1438794_x_at
Rps15a	ribosomal protein S15a	55	NM_170669	1453467_s_at
Rps20	ribosomal protein S20	47	NM_026147	1456436_x_at
Rps24	ribosomal protein S24	30	NM_011297	1436064_x_at
Rps24	ribosomal protein S24	47	NM_011297	1456628_x_at
Rps25	ribosomal protein S25	56	NM_024266	1451068_s_at
Rps3	ribosomal protein S3	44	NM_012052	1435151_a_at
Rps3	ribosomal protein S3	74	NM_012052	1447563_at
Rps6	ribosomal protein S6	66	NM_009096	1453466_at
Rps6	ribosomal protein S6	21	NM-009096	1454620_x_at
Rps6	ribosomal protein S6	43	NM_009096	1434377_x_at
Rps6	ribosomal protein S6	60	NM_00906	1435817_x_at
Rps8	ribosomal protein S8	49	NM_009098	1436760_a_at
Rps9	ribosomal protein S9	47	NM_029767	1433689_s_at
Rps9	ribosomal protein S9	21	NM_029767	1434624_x_at
Ubap2l	ubiquitin associated protein 2-like	64	NM_028475	1454643_at
Ube3a	ubiquitin protein ligase E3A	74	NM_001033962	1431224_at
Usp24	ubiquitin specific peptidase 24	73	XM_001481281	1441018_at
Usp26	ubiquitin specific peptidase 26	63	NM_031388	1421502_at
Usp27x	ubiquitin specific peptidase 27, X chromosome	77	NM_019461	1427606_at
Usp3	ubiquitin specific peptidase 3	72	NM_144937	1441056_at
Usp36	ubiquitin specific peptidase 36	72	XM_126772	1458311_at
Usp50	ubiquitin specific peptidase 50	47	NM_029163	1430760_a_at
Usp53	ubiquitin specific peptidase 53	9	NM_133857	1452385_at
Usp7	ubiquitin specific peptidase 7	46	NM_001003918	1419920_s_at
Usp9x	ubiquitin specific peptidase 9, X chromosome	46	NM_009481	1428193_at
Usp9y	ubiquitin specific peptidase 9, Y chromosome	65	NM_148943	1452509_at
Ube2v1	ubiquitin-conjugating enzyme E2 variant 1	51	NM_023230	1415755_a_at
Ube2v1	ubiquitin-conjugating enzyme E2 variant 1	17	NM_023230	1444523_s_at
Ube2f	ubiquitin-conjugating enzyme E2F (putative)	7	NM_026454	1429568_x_at
Ube2f	ubiquitin-conjugating enzyme E2F (putative)	7	NM_026454	1451272_a_at
Ube2s	ubiquitin-conjugating enzyme E2S	21	NM_133777	1430962_at

Gene symbol	Gene title	Cluster	Accession	Probe number
Ufm1	ubiquitin-fold modifier 1	21	NM_026435	1418899_at
Ubl4b	ubiquitin-like 4B	65	NM_026261	1460272_at
Uty	ubiquitously transcribed tetratricopeptide repeat gene, Y chromosome	72	NM_009484	1459565_at
Ndufa12	NADH dehydrogenase (ubiquinone) 1 alpha subcomplex, 12	64	NM_025551	1425919_at
Ndufb9	NADH dehydrogenase (ubiquinone) 1 beta subcomplex, 9	46	NM_023172	1436803_a_at
Ndufs7	NADH dehydrogenase (ubiquinone) Fe-S protein 7	51	NM_029272	1424313_a_at
Ndor1	NADPH dependent diflavin oxidoreductase 1	72	NM_001082476	1428292_at
Noxo1	NADPH oxidase organizer 1	57	NM_027988	1425151_a_at
Cybasc3	cytochrome b, ascorbate dependent 3	65	NM_201351	1454895_at
Cox6a1	cytochrome c oxidase, subunit VI a, polypeptide 1	46	NM_007748	1417417_a_at
Cox6a1	cytochrome c oxidase, subunit VI a, polypeptide 1	64	NM_007748	1417418_s_at
Cyp2c37	cytochrome P450, family 2. subfamily c, polypeptide 37	55	NM_010001	1419094_at
Cyp2c44	cytochrome P450, family 2, subfamily c, polypeptide 44	40	NM_001001446	1424576_s_at
Cyp26a1	cytochrome P450, family 26, subfamily a, polypeptide 1	78	NM_007811	1419430_at
Cyp27a1	cytochrome P450, family 27, subfamily a, polypeptide 1	6	NM_024264	1457665_x_at
Cyb5r2	cytochrome b5 reductase 2	15	NM_177216	1459448_at
Cyb5r3	cytochrome b5 reductase 3	66	NM_029787	1422186_s_at
Cyb5r3	cytochrome b5 reductase 3	61	NM_029787	1430734_at
Uqcrq	ubiquinol-cytochrome c reductase, complex III subunit VII	20	NM_025352	1427880_at
Rc3h2	ring finger and CCCH-type zinc finger domains 2	72	NM_001100591	1426925_at
Rnf11	ring finger protein 11	46	NM_013876	1452058_a_at
Rnf12	ring finger protein 12	78	NM_011276	1440850_at
Rnf138	ring finger protein 138	17	NM_019706	1419368_a_at
Rnf144b	ring finger protein 144B	8	NM_146042	1443252_at
Rnf166	ring finger protein 166	64	NM_001033142	1448079_at
Rnf170	ring finger protein 170	69	NM_029965	1434956_at
Rnf180	ring finger protein 180	71	NM_027934	1453857_at
Rnf180	ring finger protein 180	81	NM_027934	1438306_at
Rnf185	Ring finger protein 185	33	NM_145355	1459877_x_at
Rnf187	ring finger protein 187	33	XM_905766	1423896_a_at
Rnf213	Ring finger protein 213	75	NM_001040005	1460018_at
Rnf4	ring finger protein 4	17	NM_011278	1423654_a_at
Rnf41	ring finger protein 41	39	NM_026259	1432003_a_at
Rnf168	ring fnger protein 168	73	NM_027355	1455586_at

* Genes were clustered into 81 independent groups according to the overall temporal pattern of expression.